Diagn Interv Radiol 2022; DOI: 10.5152/dir.2022.211034

ARTIFICIAL INTELLIGENCE AND INFORMATICS

ORIGINAL ARTICLE

Radiomics signature for predicting postoperative disease-free survival of patients with gastric cancer: development and validation of a predictive nomogram

Shuguang Shi
Zhongchang Miao
Ying Zhou
Chunling Xu
Xue Zhang

PURPOSE

Radiomics can be used to determine the prognosis of gastric cancer (GC). The objective of this study was to predict the disease-free survival (DFS) after GC surgery based on computed tomography-enhanced images combined with clinical features.

METHODS

Clinical, imaging, and pathological data of patients who underwent gastric adenocarcinoma resection from June 2015 to May 2019 were retrospectively analyzed. The primary outcome was DFS. Radiomics features were selected using Least Absolute Shrinkage and Selection Operator algorithm and converted into the Rad-score. A nomogram was constructed based on the Rad-score and other clinical factors. The Rad-score and nomogram were validated in the training and validation groups.

RESULTS

Totally, 179 patients were randomly divided into the training (n = 124) and validation (n = 55) groups. In the training group, validation group, and overall population, the Rad-score could be divided into categories indicating low, moderate, and high risk of recurrence, metastasis, or death; all risk categories showed a significant difference between the training, validation, and overall population groups (all $P < .001$). Positive lymph nodes (hazard ratio (HR) = 3.07, 95% CI: 1.52-6.23, $P = .002$), cancer antigen-125 (HR = 3.24, 95% CI: 1.54-6.80, $P = .002$), and the Rad-score (HR = 0.73, 95% CI: 0.61-0.87, $P < .001$) were independently associated with DFS. These 3 variables were used to construct a nomogram. In the training group, the areas under the curve at 3 years were 0.758 and 0.776 for the Rad-score and the nomogram, respectively, while they were both 1.000 in the validation group. The net benefit rate was analyzed using a decision curve in the training and validation groups, and the nomogram was superior to the single Rad-score.

CONCLUSION

Rad-score is an independent factor for DFS after gastrectomy for GC. The nomogram established in this study could be an effective tool for the clinical prediction of DFS after gastrectomy.

Gastric adenocarcinomas are the most common type of stomach cancer.[1,2] There are 1 033 701 new gastric cancer (GC) cases and 872 685 GC-related deaths worldwide in 2018.[3] Some regions including Eastern Asia, Eastern Europe, and South America have the highest incidence of GC.[2,4] The treatment management of GC includes surgery, chemotherapy, radiation therapy, and targeted therapy.[1,4,5] The 5-year survival of GC patients with localized, regional, and distant-stage diseases are 67%, 31%, and 5%, respectively.[1,4,5]

The classical prognostic factors for GC include tumor size, lymphovascular invasion, nodal involvement, positive peritoneal cytology, signet ring cell adenocarcinoma,[1,2,4] age, sex,[6] and obesity.[7,8] TNM (T: primary tumor, N: lymph node, M: distant metastasis) staging system and histopathological classification have been widely used as the prognostic tools for GC, which can help to formulate the treatment strategy.[1,4,5] However, their predictive ability remains limited.[9-11] Novel prognostic biomarkers are also being explored, with similar restrictions.[12-14] In recent years, several functional imaging methods such as computed tomography (CT) perfusion, diffusion-weighted imaging (DWI), and dynamic contrast-enhanced magnetic resonance imaging have been developed. The stomach is a hollow

From the Department of Radiology (S.S., Z.M. ✉ lygzhchmiao@163.com, Y.Z., C.X., X.Z.), First people's Hospital of Lianyungang, First Affiliated Hospital of Kangda College of Nanjing Medical University, Lianyungang, Jiangsu, China.

Received 20 October 2021; revision requested 27 December 2021; last revision received 19 March 2022; accepted 18 April 2022.

Publication date: 26 August 2022.

DOI: 10.5152/dir.2022.211034

You may cite this article as: Shi S, Miao Z, Zhou Y, Xu C, Zhang X. Radiomics signature for predicting postoperative disease-free survival of patients with gastric cancer: development and validation of a predictive nomogram. *Diagn Interv Radiol.* 2022;28(5):441-449.

moving organ filled with liquid and gas, and its motion may exacerbate artifacts, resulting in image distortion and ghosting. In addition, concerning the DWI sequence, susceptibility artifacts, distortions, and blurring are inevitable due to the slow traversal through the k-space line and the narrow bandwidth along the phase encoding direction.[15] Among them, emerging radiomics is a promising prognostic tool for GC. Radiomics signatures, which compose of a series of CT texture features, are considered to be a stronger predictive factor, providing additional information beyond the traditional clinical factors.[16,17]

Previous studies examined the predictive value of radiomics in GC prognosis. A study showed that radiomics could predict recurrence-free survival (RFS) in locally advanced GC.[18] Another radiomics-based model could predict lymphovascular invasion and progression-free survival (PFS) but not overall survival (OS).[19] However, GC radiomics is still in its infancy, facing multiple challenges.[20]

Therefore, this study aimed to predict the disease-free survival (DFS) after GC surgery based on preoperative CT-enhanced images combined with clinical features. The results may help to improve the ability to predict DFS after gastrectomy.

Methods

Study design and patient data

This retrospective study analyzed the clinical, imaging, and pathological data of patients who underwent gastric adenocarcinoma resection from June 2015 to May 2019. The study was approved by the Ethics Committee. The decision number of Ethics Committee approval is LW-20220210001-01.

All patients were pathologically diagnosed with gastric adenocarcinoma according to the 2010 World Health Organization (WHO) Classification of Tumours of the Digestive System.[21] The inclusion criteria

Main points

- Rad-score is an independent factor for disease-free survival (DFS) after gastrectomy for gastric cancer.
- Rad-score could be divided into categories indicating low, moderate, and high risk, and each category was associated with distinct DFS.
- Nomogram could be an effective tool for the clinical prediction of DFS after gastrectomy.

Table 1. Characteristics of the patients

General characteristics	Total (n = 179)	Training (n = 124)	Validation (n = 55)	*P*
Age (year)				.062
≤60 years	67 (37.4%)	38 (30.6%)	29 (52.7%)	
>60 years	112 (62.6%)	86 (69.4%)	26 (47.3%)	
Sex				.961
Male	129 (72.1%)	90 (72.6%)	39 (70.9%)	
Female	50 (27.9%)	34 (27.4%)	16 (29.1%)	
CEA				.765
≤5 ng/mL	145 (81.0%)	107 (86.3%)	38 (69.1%)	
>5 ng/mL	34 (19.0%)	17 (13.7%)	17 (30.1%)	
CA-125				.359
≤35 U/mL	156 (87.2%)	107 (86.3%)	49 (89.1%)	
>35 U/mL	23 (12.8%)	17 (13.7%)	6 (10.9%)	
CA-199				.537
≤27 U/mL	133 (74.3%)	93 (75.0%)	40 (72.7%)	
>27 U/mL	46 (25.7%)	31 (25.0%)	15 (27.3%)	
CA-153				.764
≤25 U/mL	164 (91.6%)	112 (90.3%)	52 (94.5%)	
>25 U/mL	15 (8.4%)	12 (9.7%)	3 (5.5%)	
NSE				.712
≤16 ng/mL	163 (91.1%)	111 (89.5%)	52 (94.5%)	
>16 ng/mL	16 (8.9%)	13 (10.5%)	3 (5.5%)	
Maximal diameter of the tumor				.538
≤30 mm	41 (22.9%)	30 (24.2%)	11 (20.0%)	
>30 mm	138 (77.1%)	94 (75.8%)	44 (80.0%)	
Thickness of the tumor				.772
≤20 mm	98 (54.7%)	67 (54.0%)	31 (56.4%)	
>20 mm	81 (45.3%)	57 (46.0%)	24 (43.6%)	
Internal necrosis	172 (96.1%)	119 (96.0%)	53 (96.4%)	.9
Borrmann classification				.627
Type I	0	0	0	
Type II	19 (10.6%)	15 (12.1%)	4 (7.3%)	
Type III	72 (40.2%)	49 (39.5%)	23 (41.8%)	
Type IV	88 (49.2%)	60 (48.4%)	28 (50.9%)	
Tumor location				.578
Cardia	44 (24.6%)	33 (26.6%)	11 (20%)	
Body	23 (12.8%)	17 (13.7%)	6 (10.9%)	
Antrum	83 (46.4%)	56 (45.2%)	27 (49.1%)	
Whole	29 (16.2%)	18 (14.5%)	11 (20%)	
cT staging				.905
cT1	1 (0.6%)	1 (0.8%)	0	
cT2	22 (12.3%)	15 (12.1%)	7 (12.7%)	
cT3	62 (34.6%)	42 (33.9%)	20 (36.4%)	
cT4	94 (52.5%)	66 (53.2%)	28 (50.9%)	

(*Continued*)

Table 1. Characteristics of the patients (*Continued*)

General characteristics	Total (n = 179)	Training (n = 124)	Validation (n = 55)	*P*
cN staging				.743
Negative	65 (36.3%)	46 (37.1%)	19 (34.5%)	
Positive	114 (63.7%)	78 (62.9%)	36 (65.5%)	
pT staging				.988
T1	5 (2.8%)	4 (3.2%)	1 (1.8%)	
T2	23 (12.8%)	17 (13.7%)	6 (10.9%)	
T3	66 (36.9%)	46 (37.1%)	20 (36,4%)	
T4	85 (47.5%)	57 (46.0%)	28 (50.9%)	
Differentiation degree				.667
Poor	113 (63.1%)	79 (63.7%)	34 (61.8%)	
Moderate	53 (29.6%)	35 (28.2%)	18 (32.7%)	
Well-differentiated	13 (7.3%)	10 (8.1%)	3 (5.5%)	
Lymph node metastasis	115 (64.2%)	77 (62.1%)	38 (69.1%)	.98
CD34-positive	136 (76.0%)	91 (73.4%)	45 (81.8%)	.141
HER-2-positive	87 (48.6%)	62 (50.0%)	25 (45.5%)	.368
VEGF				.771
Negative	23 (12.8%)	16 (12.9%)	7 (12.7%)	
Weakly positive	48 (26.8%)	34 (27.4%)	14 (25.5%)	
Strongly positive	108 (60.3%)	74 (59.7%)	34 (61.8%)	
EGFR				.485
Negative	26 (14.5%)	18 (14.5%)	8 (14.5%)	
Weakly positive	66 (36.9%)	40 (32.3%)	26 (47.3%)	
Strongly positive	87 (48.6%)	66 (53.2%)	21 (38.2%)	
Ki-67 index				.918
≤50%	52 (29.1%)	35 (28.2%)	17 (30.9%)	
>50%	127 (70.9%)	89 (71.8%)	38 (69.1%)	
Adjuvant treatment	116 (64.8%)	81 (65.3%)	35 (63.6%)	.532
Recurrence, metastasis, or all-cause death	84 (46.9%)	58 (46.8%)	26 (47.3%)	.465

CEA, carcinoembryonic antigen; CA, cancer antigen; NSE, neuron-specific enolase; VEGF, vascular endothelial growth factor; EGFR, epithelial growth factor receptor.

were (1) diagnosis of gastric adenocarcinoma by pathological examination, (2) complete clinical, imaging, and pathological data, (3) no anti-tumor treatment before CT examination, and (4) radical GC surgery within 2 weeks after CT examination. The exclusion criteria were (1) poor image quality, (2) the lesion being too small to delineate the region of interest (ROI), or (3) follow-up <6 months.

The included patients were randomly divided into the training and validation groups in a 2 : 1 ratio.

Follow-up

GC patients were followed up routinely every 3 months during the first 2 years after surgery and every 6 months thereafter. Follow-up was censored on May 30, 2019. Routine follow-up included laboratory examinations (carcinoembryonic antigen (CEA), cancer antigen (CA)-125, CA-199, etc.) and imaging examinations (CT plain and enhanced scans), positron emission tomography-CT, and magnetic resonance imaging if deemed necessary.

The primary outcome was DFS. DFS was defined as the period from the first postoperative day to tumor recurrence, diagnosis of metastasis, or all-cause death, whichever occurred first.

Observational indicators

Clinical factors that might be related to DFS included sex, age, pathological diagnosis, histological differentiation, depth of invasion, number of metastatic lymph nodes, tumor markers (CEA, CA-125, CA-199, CA-153, and neuron-specific enolase), and immunohistochemistry staining results for CD34, vascular endothelial growth factor, epidermal growth factor receptor, and Human epidermal growth factor receptor-2 (HER-2) (0 = negative, 1 = weakly positive, and 2 = strongly positive), Ki-67 index, and adjuvant treatment. Histological differentiation was classified into well-differentiated, highly moderately differentiated, moderately differentiated, moderately poorly differentiated, and poorly differentiated. The postoperative pathological staging was determined according to the standards stated in the eighth edition of American Joint Committee on Cancer.

There were several forms of adjuvant treatment. We considered these adjuvant treatments had effects on DFS, so we considered the adjuvant treatment as one variable.

The basic imaging features that might be related to DFS included tumor size (maximum diameter of the largest cross-section, mm), internal tumor necrosis, tumor thickness (thickness of the largest cross-section, mm) Borrmann classification of tumor types (type I-protruding type, type II-superficial ulcerative type, III-ulcer-infiltrating type, and type IV-diffuse infiltrative type), preoperative primary tumor staging (cT staging), and preoperative lymph node staging (cN staging). Two attending radiologists who, respectively, had 10 and 6 years of experience in abdominal imaging diagnosis and were unaware of the contents of the study evaluated the basic imaging characteristics of the included patients. When the assessment results were inconsistent, a chief radiologist with 20 years of experience in abdominal CT diagnosis made the final decision.

CT examination

Food and water were prohibited for 12 hours. Ten minutes before the examination, 15 mg of anisodamine was injected intramuscularly to reduce gastric motility, and 1200 mL of water was drunk to expand the gastric cavity. During the examination, after a plain scan in the supine position, 80 mL of radiocontrast agent (Ultravist 370, Bayer) was injected through the median cubital vein at 3.0 mL/s (High-Pressure Injector, CT Plus 150, Ulrich Medical). The

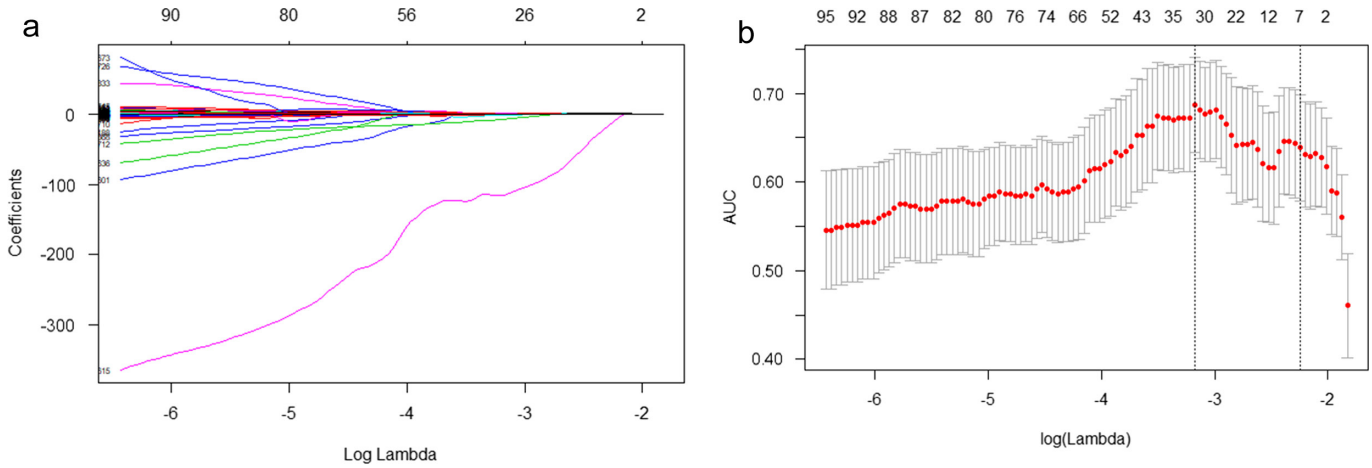

Figure 1. a, b. LASSO regression model for screening the radiomics characteristics of the training group. **(a)** The vertical axis represents the coefficients corresponding to 776 radiomics characteristics, and the horizontal axis represents logλ. **(b)** The vertical axis represents the corresponding AUC, and the horizontal axis represents logλ. In the LASSO program, n lamada = 100, n folds = 10, and the minimum multiple of 1 standard deviation is used. LASSO, Least Absolute Shrinkage and Selection Operator algorithm; AUC, area under the curve.

scan ranged from the diaphragmatic dome to the anterior superior iliac spine. The arterial phase images were collected 30 seconds after the injection of the radiocontrast agent, and the portal vein phase images were collected at 65 seconds. The scanned CT images were exported from the Picture Archiving and Communication System system and workstation in Digital Imaging and Communications in Medicine format. The CT machine with a 64 LightSpeed VCT (GE Healthcare) or SOMATOM Definition Dual Source CT (Siemens) was adopted.

Extraction of textural features

The image data of the arterial and portal venous phases with reconstructed layers thicknesses of 5 and 1.25 mm were exported. A radiologist with 6 years of experience used the open-source software 3D Slicer (http://www.slicer.org Version:4.10.2) to draw an ROI on the stomach lesion in which the largest layer was selected, paying attention to exclude adjacent gas and fat. The gray value in the ROI was analyzed using the radiomics plug-in in 3D Slicer. Radiologist A had 6 years of experience in abdominal CT diagnosis and 2 years of experience in textural feature extraction, and radiologist B had 10 years of experience in abdominal

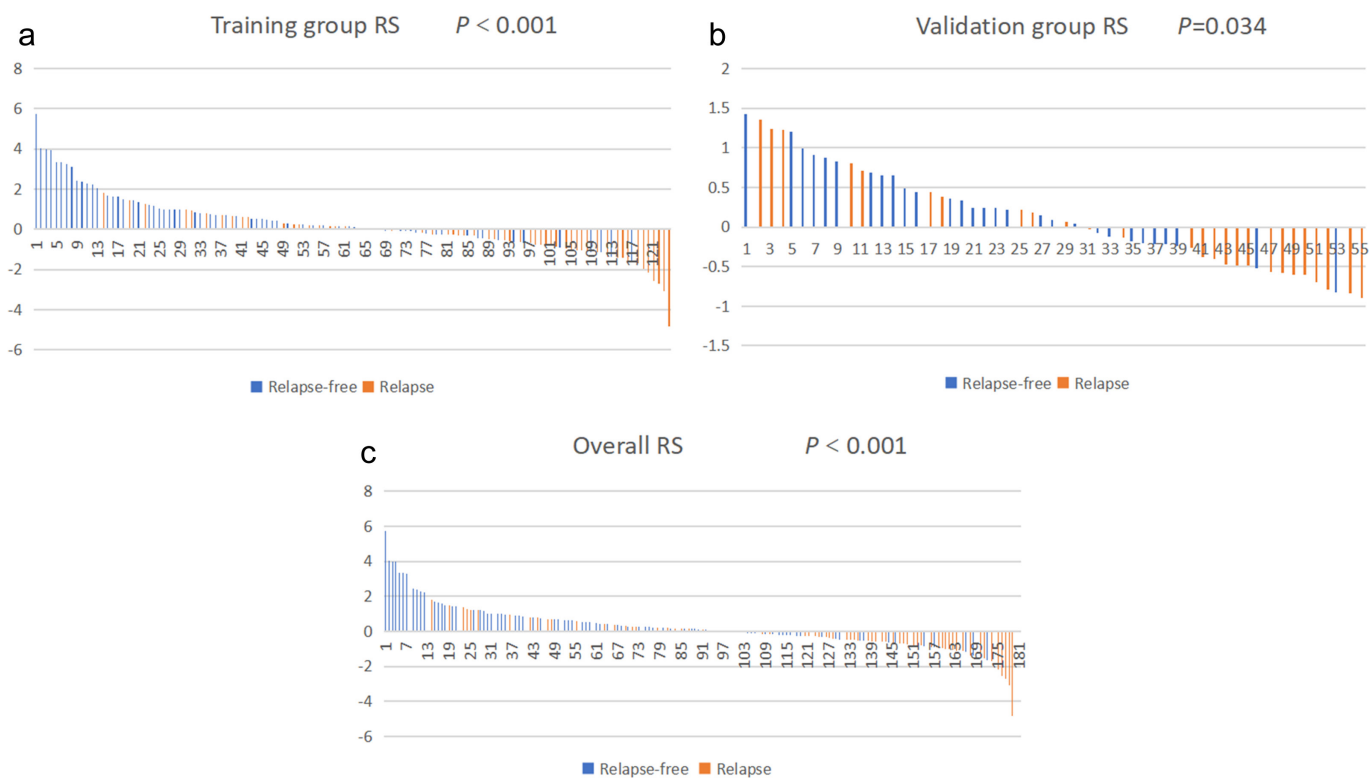

Figure 2. a-c. Comparison between the Rad-score of recurrence/metastasis and the Rad-score of no recurrence/metastasis of the training group **(a)**, the validation group **(b)**, and the overall study population **(c)**. *Red* indicates that the patient has recurrence/metastasis. *Blue* indicates the patient has no recur rence/metastasis. The vertical axis indicates the Radiomics score (RS) score.

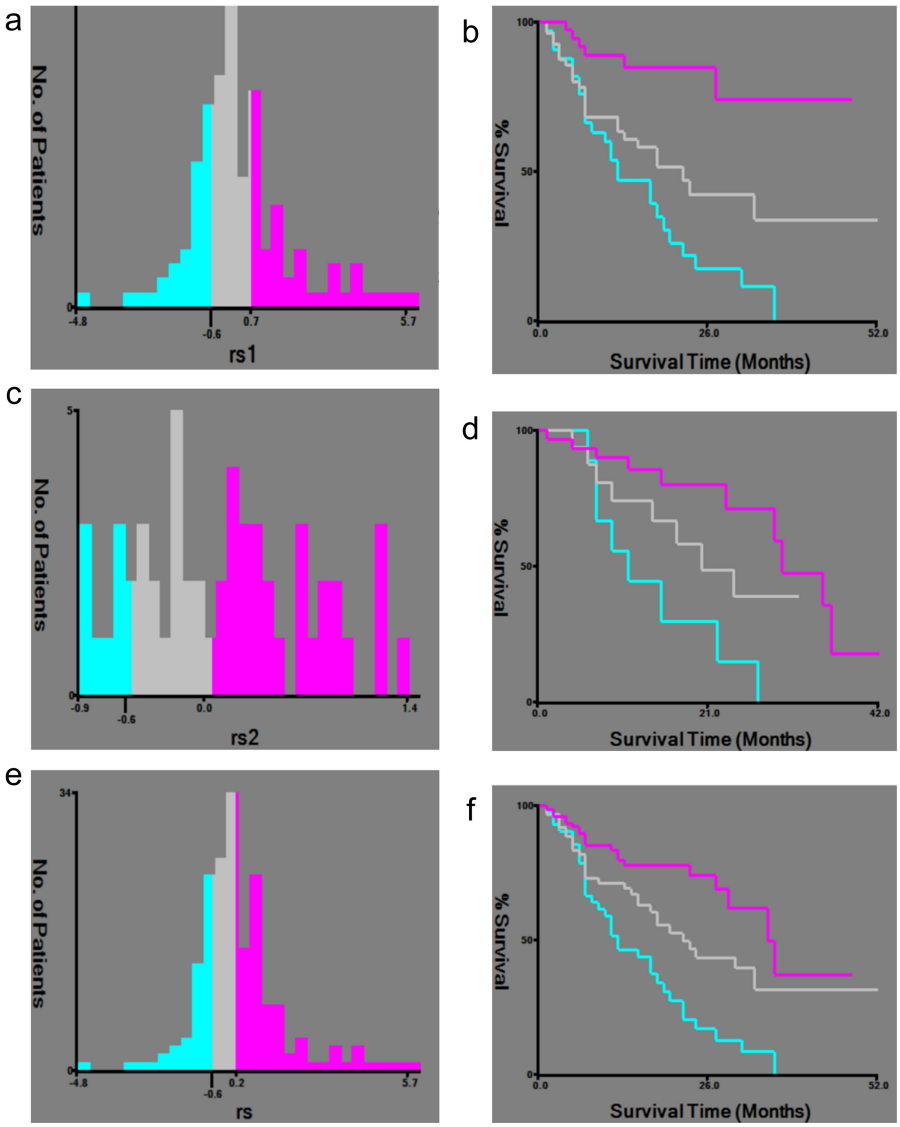

Figure 3. a-f. (a-b) Use of X-tile to predict the best Rad-score value of DFS in the training group (n = 124). **(c-d)** Use of X tile to predict the best Rad-score value of DFS in the validation group (n = 55). **(e-f)** Use of X-tile to predict the best Rad-score value of DFS of all cases (n = 179). *Pink* means cases with low risk of recurrence/metastasis/death, *blue* means cases with high risk of recurrence/metastasis/death, and *grey* means cases with moderate risk of recurrence/metastasis/death. DFS, disease-free survival.

CT diagnosis and 1 year of experience in textural feature extraction. They randomly selected the venous phase imaging data of 30 cases, with a layer thickness of 1.25 mm, and performed lesion ROI delineation and textural feature extraction independently without knowing the research content and clinical data. Radiologist A performed feature extraction again on the same image 1 month later to evaluate its repeatability and then completed feature extraction of other image data.

Surgical procedure

The surgical procedures for GC included Billroth I and II gastrojejunostomy, Roux-en-Y hepaticojejunostomy, and others, as listed in Table 5.

Statistical analysis

In the training group, Least Absolute Shrinkage and Selection Operator (LASSO) algorithm was used in dimensionality reduction of the features to select the textural features that could predict the DFS. The selected minimum textural feature value was multiplied by the corresponding coefficient to obtain the radiomics score (Rad-score). According to the case status (recurrence, metastasis, or death) and DFS time, the X-tile software was used to calculate the cutoff value of the Rad-score. The relationship between the Rad-score and DFS was evaluated through Kaplan–Meier survival analysis. The patients were divided into the high-, moderate-, and low-risk groups based on the Rad-score value.

In the training group, univariable analysis was performed on the included clinical features (categorical variables) using the Cox survival analysis. Variables with $P < .05$ were included in the Cox multivariable analysis (forward stepwise). Variables left in the final equation were used to establish a predictive nomogram. The time-dependent receiver operating characteristics (ROC) curves and decision curves were drawn to evaluate the predictive ability of the nomogram.

Categorical data were presented as n (%) and analyzed using the chi-square test or Fisher exact test. The statistical software used included R 3.0.1, X-tile 3.6.1 (https://medicine.yale.edu/lab/rimm/research/software), and Statistical Package for the Social Sciences software 26.0 (IBM). A two-sided *P*-value < .05 was considered statistically significant.

Results

From June 2015 to May 2019, 654 patients underwent gastric adenocarcinoma resection. Among them, 179 patients met the eligibility criteria and were randomly divided into the training (n = 124) and validation (n = 55) groups. There were no statistically significant differences between the 2 groups (Table 1).

In the training group, 7 features with a non-zero coefficient were selected through the LASSO regression model, as shown in Figure 1. Based on these 7 features, the Rad-score was constructed as the following equation:

Rad-score = 11.581 − 0.009 × original_shape_Maximum 2D Diameter Column − 0.252×original_glrlm_RunEntropy + 0.002× original_glrlm_Run Length NonUniformity Normalized − 0.257 × square_firstorder_Skewness − 0.805 × wavelet-HLH_glszm_Zone Entropy − 11.540 × wavelet-HHH_glcm_Sum Squares + 1.067 × wavelet-HHL_glrlm_Run Length NonUniformity Normalized.

In the training group, validation group, and overall population, the Rad-score of the recurrence/metastasis group and the non-recurrence/metastasis group was compared (Figure 2). In addition, Rad-score could be divided into different categories indicating low, moderate, and high risk of

recurrence, metastasis, or death (Figure 3 and Supplementary Tables S1-S3). The Rad-scores in all risk categories were significantly different (all $P < .001$) between the training, validation, and overall population groups.

Table 2 shows that the Rad-score ($P < .001$), CA-125 ($P = .010$), maximal diameter of the tumor ($P = .018$), thickness of the tumor ($P = .002$), Borrmann classification ($P = .008$), cT staging ($P = .001$), cN staging ($P = .007$), pT staging ($P = .006$), differentiation degree ($P = .026$), positive lymph nodes ($P = .002$), and positive-CD34 ($P = .043$) are associated with DFS in the univariable analysis. Multivariable analysis showed that positive lymph nodes (hazard ratio (HR) = 3.07, 95% CI: 1.52-6.23, $P = .002$), CA-125 (HR = 3.24, 95% CI: 1.54-6.80, $P = .002$), and Rad-score (HR = 0.73, 95% CI: 0.61-0.87, $P < 0.001$) were independently associated with DFS (Table 3).

Table 2. Univariable analysis of DFS in the training group

Variables	HR (95% CI)	*P*
Rad-score	0.700 (0.588-0.833)	<.001
Age	1.039 (0.598-1.804)	.893
Sex	0.935 (0.519-1.684)	.823
CEA	0.828 (0.392-1.751)	.621
CA-125	0.389 (0.189-0.800)	.010
CA-199	1.770 (0.915-3.422)	.090
CA-153	1.658 (0.783-3.512)	.187
NSE	0.663 (0.240-1.834)	.429
Maximal diameter of the tumor	2.461 (1.165-5.201)	.018
Thickness of the tumor	2.353 (1.383-4.001)	.002
Internal necrosis	3.151 (0.436-22.784)	.255
Borrmann classification	1.750 (1.159-2.641)	.008
cT staging	2.060 (1.340-3.166)	.001
cN staging	2.298 (1.258-4.200)	.007
pT staging	1.678 (1.163-2.420)	.006
Differentiation degree	0.581 (0.360-0.936)	.026
Lymphatic metastasis	2.653 (1.427-4.931)	.002
CD34	2.084 (1.023-4.244)	.043
HER-2	1.489 (0.884-2.508)	.135
VEGF	1.073 (0.749-1.536)	.702
EGFR	1.283 (0.892-1.845)	.179
Ki-67 Index	1.076 (0.604-1.916)	.803
Adjuvant treatment	1.462 (1.109-3.471)	.179

HR, hazard ratio; CEA, carcinoembryonic antigen; CA, cancer antigen; NSE, neuron-specific enolase; VEGF, vascular endothelial growth factor; EGFR, epithelial growth factor receptor.

Table 3. Multivariable analysis of the risk factors affecting DFS in the training group

Risk factor	HR (95% CI)	*P*
Lymphatic metastasis	3.074 (1.518-6.227)	.002
CA-125	3.239 (1.542-6.804)	.002
Rad-score	0.726 (0.605-0.872)	<.001

HR, hazard ratio; CA, cancer antigen.

In the training group, a nomogram based on 2 clinical variables and the Rad-score was constructed, as shown in Figure 4. The time-dependent ROC curve verification was performed in the training and validation groups. In the training group, the areas under the curve (AUCs) at 3 years were 0.758 and 0.776 for the Rad-score and the nomogram, respectively, while they were both 1.000 in the validation group (Figure 5 and Table 4).

The net benefit rate was analyzed using a decision curve in the training and validation groups. Compared with the Rad-score alone, the net benefit of the nomogram showed better predictive ability (Figure 6).

ROC curve analysis was performed to assess the predictive capability of the Rad-score, clinical model (incorporating lymphadenopathy and CA-125), and the combined model of the training group. The

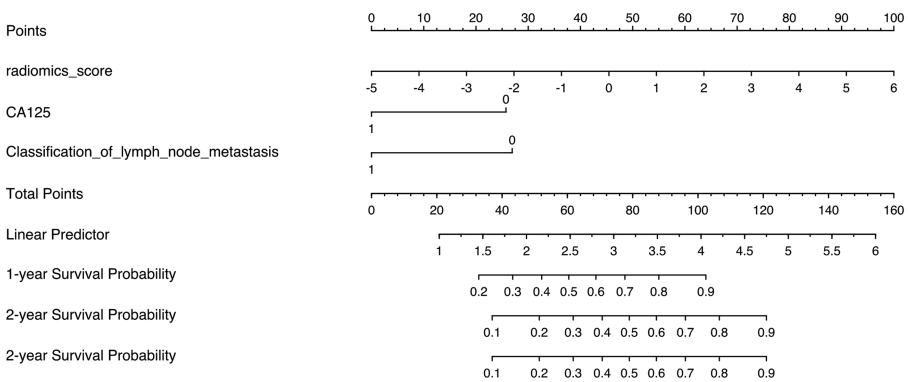

Figure 4. Disease-free survival risk estimation based on the Rad-score and the nomogram of other risk factors in the training group. CA, cancer antigen.

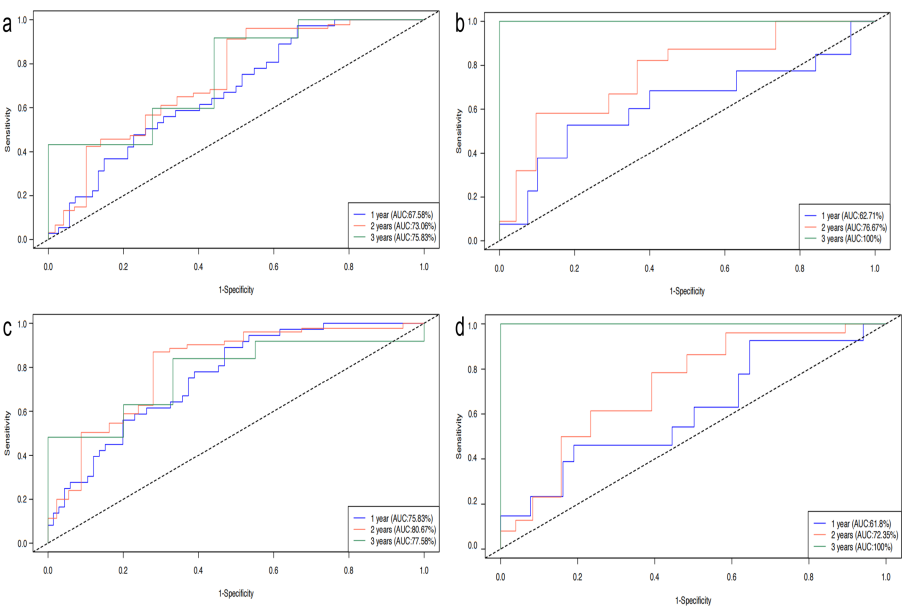

Figure 5. a-d. (a) Time-dependent receiver operating characteristic curves of the Rad-score in the training group. **(b)** Time-dependent ROC curves of Rad-score in the validation group. **(c)** Time-dependent ROC curves of nomogram in the training group. **(d)** Time-dependent ROC curves of nomogram in the validation group. ROC, receiver operating characteristic.

Table 4. AUCs of the Rad-score and the nomogram		
Dataset	Rad-score	Nomogram
Training group		
1-year DFS	0.676	0.758
2-year DFS	0.730	0.807
3-year DFS	0.758	0.776
Validation group		
1-year DFS	0.627	0.618
2-year DFS	0.767	0.724
3-year DFS	1.000	1.000

AUC, area under the curve; DFS, disease-free survival.

to predict DFS after GC surgery based on CT-enhanced images combined with clinical features. The results suggested that the Rad-score was an independent predictive factor for DFS after gastrectomy. The nomogram could be an effective tool for the clinical prediction of DFS after gastrectomy.

Radiomics has been explored for the differential diagnosis of GC and the prediction of its histological grade, tumor stage, response to therapy, and prognosis.[20] Shin et al.[18] showed that radiomics could predict RFS in patients with locally advanced GC. Chen et al.[19] developed a radiomics-based model that could predict lymphovascular invasion and PFS but not OS. In postoperative patients, Giganti et al.[22] identified image features associated with a poor prognosis. Li et al.[23] used the LASSO method to identify features included in a Cox model for the prediction of OS. In the present study, the LASSO method was also used to identify 7 image features that could be used to build the Rad-score. Then, the Rad-score could be divided into categories indicating low, moderate, and high risk, and each category was associated with distinct DFS. Previous studies also reported that radiomics signatures could be stratified based on risk levels, offering a prognostic value.[24-27]

Still, radiomics alone might not be the best predictor for GC prognosis, and its combination with traditional clinical prognostic factors might improve its predictive ability. Indeed, in the present study, positive lymph nodes and CA-125 were found to be independently associated with DFS along with the Rad-score. The presence of positive lymph nodes is a well-known poor prognostic factor for solid cancers, including GC.[1,4,5,28,29] CA-125 is also associated with the prognosis of GC.[30,31] According to the WHO 2019 classification,[32] some of the selected changes in the new classification results showed that the AUC of the combined model was higher than that of the clinical model (Figure 7).

The different forms of surgical procedure and adjuvant treatment are listed in Table 5 and Table 6.

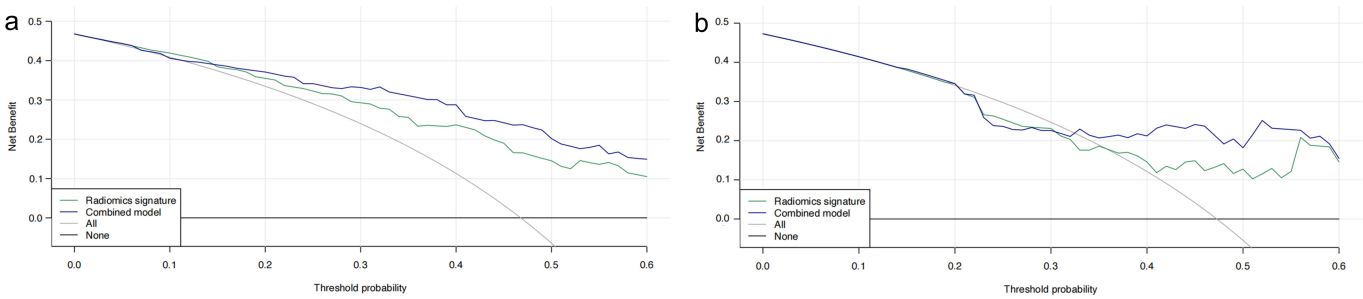

Figure 6. a, b. (a) Net benefit rate analyzed via the decision curve of the training group. **(b)** Net benefit rate analyzed via the decision curve of the validation group.

Discussion

Radiomics can be used to determine the prognosis of GC.[18-20] This study aimed

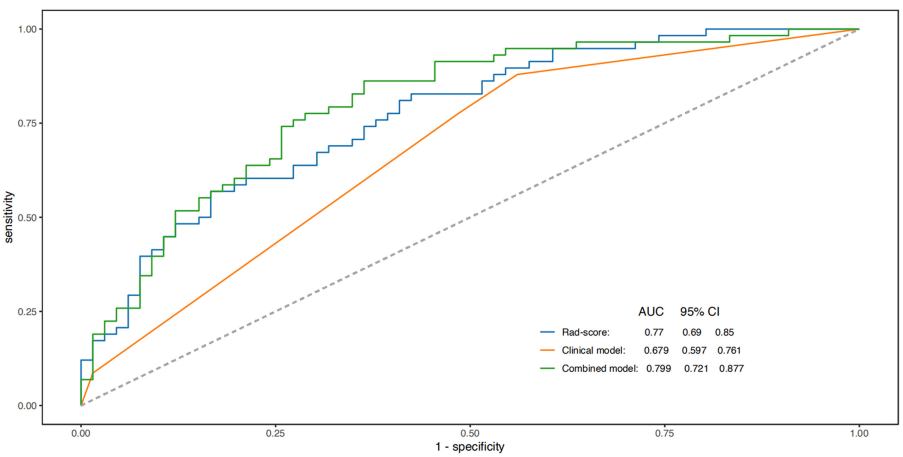

Figure 7. ROC analysis of Rad-score, clinical model (including lymphadenopahy and CA-125) and the combined model of training group shows that the AUC of the combined model was higher than that of the clinical model.

Table 5. Surgical procedure	
Surgical procedure	Number (n)
Distal gastrectomy (Roux-en-Y procedure)	38
Proximal gastrectomy	9
Subtotal gastrectomy (Billroth I)	19
Subtotal gastrectomy (Billroth II)	14
Total gastrectomy with esophagojejunostomy	76
Laparoscopic gastrectomy	12
Gastroscopic cardia resection	11

Table 6. Different forms of adjuvant treatment	
Forms of adjuvant treatment	Number (n)
Postoperative chemotherapy	84
Postoperative chemotherapy and targeted therapy	12
Postoperative chemotherapy and radiotherapy	2
Postoperative targeted therapy	1
Preoperative neoadjuvant chemotherapy and postoperative chemotherapy	17
Total	116

of GC-related digestive system tumors are microsatellite instability high (MSI-H) and Epstein-Barr virus (EBV) positivity, which are good prognostic markers with potential therapeutic importance that can be used in future radiomic studies. MSI-H GC[33] is characterized by a predisposition to older age and female gender, distal location, and better survival. Moore et al.[34] indicated that EBV subtype was more prevalent in young-onset GC and might play a key role in the pathogenesis of GC, so our study might further prove this finding.

The nomogram constructed using the 3 variables had a better predictive ability than the Rad-score alone. Li et al.[23] combined their radiomics signature with traditional prognostic factors (T stage, N stage, and histological differentiation) and showed improved predictive ability compared with radiomics alone. Similar results were also observed by Wang et al.[24] using a nomogram that included a radiomics signature, extramural vessel invasion, cT stage, and cN stage and by Zhang et al.[35] using radiomics, cN stage, CA-199, CEA, and Borrmann type. Differences in the clinical factors included in the nomograms could be influenced by the characteristics of the populations in different studies. ROC curve analysis of Rad-score, clinical model, and combined model of training group showed that the predictive ability of the combined model was higher than that of the clinical model, so the addition of the Rad-score increased the prognostic power for DFS in comparison with the clinical model.

However, radiomics faces challenges in its wide-scale application. Indeed, the models are highly dependent on image acquisition, image segmentation, feature extraction and selection, and model construction and validation. Variations in scanners, layer thickness, acquisition parameters, and reconstruction parameters will affect the radiomics features.[36-40] In addition, image segmentation based on either ROI or voxels of interest is usually performed manually, which can influence the results.[23,40,41] The various software available for feature extraction and weighing will influence the model.[42,43] Those issues need to be solved before radiomics-based predictive models can be widely used. Furthermore, multiple imaging modalities could be combined to acquire a more comprehensive representation image of the tumor and improve the predictive ability of the models.[17]

This study had limitations. First, this study was a single-center, retrospective study, and multicenter validation should be performed in the future. Second, due to the limited number of patients and follow-up time, OS could not be assessed. The relationship between the Rad-score and postoperative chemotherapy for gastric cancer will also have to be examined in the future.

In conclusion, the Rad-score was independently associated with DFS after gastrectomy. Its predictive ability was higher when combined with traditional clinical factors. The nomogram chart established in our study could be an effective tool for clinical prediction of DFS after gastrectomy.

Conflict of interest disclosure

The authors declared no conflicts of interest.

References

1. NCCN Clinical Practice Guidelines in Oncology (NCCN Guidelines). *Gastric Cancer*. Version 3.2021. Fort Washington: National Comprehensive Cancer Network; 2021.
2. Van Cutsem E, Sagaert X, Topal B, Haustermans K, Prenen H. Gastric cancer. *Lancet*. 2016;388(10060):2654-2664. [CrossRef]
3. Bray F, Ferlay J, Soerjomataram I, Siegel RL, Torre LA, Jemal A. Global cancer statistics 2018: GLOBOCAN estimates of incidence and mortality worldwide for 36 cancers in 185 countries. *CA Cancer J Clin*. 2018;68(6):394-424. [CrossRef]
4. Smyth EC, Verheij M, Allum W, et al. Gastric cancer: ESMO clinical practice guidelines for diagnosis, treatment and follow-up. *Ann Oncol*. 2016;27(suppl 5):v38-v49. [CrossRef]
5. Japanese Gastric Cancer Association. Japanese gastric cancer treatment guidelines 2018 (5th edition). *Gastric Cancer*. 2021;24(1):1-21. [CrossRef]
6. Kim JH, Boo YJ, Park JM, et al. Incidence and long-term outcome of young patients with gastric carcinoma according to sex: does hormonal status affect prognosis? *Arch Surg*. 2008;143(11):1062-1067. [CrossRef]
7. Ojima T, Iwahashi M, Nakamori M, et al. Influence of overweight on patients with gastric cancer after undergoing curative gastrectomy: an analysis of 689 consecutive cases managed by a single center. *Arch Surg*. 2009;144(4):351-358. [CrossRef]
8. Lee JH, Park B, Joo J, et al. Body mass index and mortality in patients with gastric cancer: a large cohort study. *Gastric Cancer*. 2018;21(6):913-924. [CrossRef]
9. Liu JY, Peng CW, Yang XJ, Huang CQ, Li Y. The prognosis role of AJCC/UICC 8(th) edition staging system in gastric cancer, a retrospective analysis. *Am J Transl Res*. 2018;10(1):292-303.
10. Röcken C, Behrens HM. Validating the prognostic and discriminating value of the TNM-classification for gastric cancer - a critical appraisal. *Eur J Cancer*. 2015;51(5):577-586. [CrossRef]
11. Zhu Z, Gong Y, Xu H. Clinical and pathological staging of gastric cancer: current perspectives and implications. *Eur J Surg Oncol*. 2020;46(10 Pt B):e14-e19. [CrossRef]
12. Choi YY, Bae JM, An JY, et al. Is microsatellite instability a prognostic marker in gastric cancer? A systematic review with meta-analysis. *J Surg Oncol*. 2014;110(2):129-135. [CrossRef]
13. Liu JL, Gao W, Kang QM, Zhang XJ, Yang SG. Prognostic value of survivin in patients with gastric cancer: a systematic review with meta-analysis. *PLoS One*. 2013;8(8):e71930. [CrossRef]
14. Luo Y, Zhang X, Tan Z, et al. Astrocyte elevated Gene-1 as a novel clinicopathological and prognostic biomarker for gastrointestinal cancers: a meta-analysis with 2999 patients. *PLoS One*. 2015;10(12):e0145659. [CrossRef]
15. Cai JS, Chen HY, Chen JY, et al. Reduced field-of-view diffusion-weighted imaging (DWI) in patients with gastric cancer: comparison with conventional DWI techniques at 3.0T: a preliminary study. *Med (Baltim)*. 2020;99(1):e18616. [CrossRef]
16. Lambin P, Rios-Velazquez E, Leijenaar R, et al. Radiomics: extracting more information from medical images using advanced feature analysis. *Eur J Cancer*. 2012;48(4):441-446. [CrossRef]
17. Kumar V, Gu Y, Basu S, et al. Radiomics: the process and the challenges. *Magn Reson Imaging*. 2012;30(9):1234-1248. [CrossRef]
18. Shin J, Lim JS, Huh YM, et al. A radiomics-based model for predicting prognosis of locally advanced gastric cancer in the preoperative setting. *Sci Rep*. 2021;11(1):1879. [CrossRef]
19. Chen X, Yang Z, Yang J, et al. Radiomics analysis of contrast-enhanced CT predicts lymphovascular invasion and disease outcome in gastric cancer: a preliminary study. *Cancer Imaging*. 2020;20(1):24. [CrossRef]
20. Wang Y, Jin ZY. Radiomics approaches in gastric cancer: a frontier in clinical decision making. *Chin Med J (Engl)*. 2019;132(16):1983-1989. [CrossRef]
21. Bosman FT, Carneiro F, Hruban RH, Theise ND. *WHO Classification of Tumours of the Digestive System*. Lyon: IARC Press; 2010.
22. Giganti F, Antunes S, Salerno A, et al. Gastric cancer: texture analysis from multidetector computed tomography as a potential preoperative prognostic biomarker. *Eur Radiol*. 2017;27(5):1831-1839. [CrossRef]
23. Li W, Zhang L, Tian C, et al. Prognostic value of computed tomography radiomics features in patients with gastric cancer following curative resection. *Eur Radiol*. 2019;29(6):3079-3089. [CrossRef]
24. Wang S, Feng C, Dong D, et al. Preoperative computed tomography-guided disease-free survival prediction in gastric cancer: a multicenter radiomics study. *Med Phys*. 2020;47(10):4862-4871. [CrossRef]
25. Jiang Y, Yuan Q, Lv W, et al. Radiomic signature of (18)F fluorodeoxyglucose PET/CT for prediction of gastric cancer survival and chemotherapeutic benefits. *Theranostics*. 2018;8(21):5915-5928. [CrossRef]
26. Huang Y, Liu Z, He L, et al. Radiomics signature: a potential biomarker for the prediction of disease-free survival in early-stage (I or II) non-small cell lung cancer. *Radiology*. 2016;281(3):947-957. [CrossRef]

27. Park H, Lim Y, Ko ES, et al. Radiomics signature on magnetic resonance imaging: association with disease-free survival in patients with invasive breast cancer. *Clin Cancer Res*. 2018;24(19):4705-4714. [CrossRef]
28. Deng J, Liang H, Sun D, Pan Y. The prognostic analysis of lymph node-positive gastric cancer patients following curative resection. *J Surg Res*. 2010;161(1):47-53. [CrossRef]
29. Wang H, Qi H, Liu X, et al. Positive lymph node ratio is an index in predicting prognosis for remnant gastric cancer with insufficient retrieved lymph node in R0 resection. *Sci Rep*. 2021;11(1):2022. [CrossRef]
30. Emoto S, Ishigami H, Yamashita H, Yamaguchi H, Kaisaki S, Kitayama J. Clinical significance of CA125 and CA72-4 in gastric cancer with peritoneal dissemination. *Gastric Cancer*. 2012;15(2):154-161. [CrossRef]
31. Luo T, Chen W, Wang L, Zhao H. CA125 is a potential biomarker to predict surgically incurable gastric and cardia cancer: a retrospective study. *Med (Baltim)*. 2016;95(51):e5297. [CrossRef]
32. Nagtegaal ID, Odze RD, Klimstra D, et al. The 2019 WHO classification of tumours of the digestive system. *Histopathology*. 2020;76(2):182-188. [CrossRef]
33. Yamamoto H, Perez-Piteira J, Yoshida T, et al. Gastric cancers of the microsatellite mutator phenotype display characteristic genetic and clinical features. *Gastroenterology*. 1999;116(6):1348-1357. [CrossRef]
34. Moore A, Hikri E, Goshen-Lago T, et al. Young-onset gastric cancer and Epstein-Barr virus (EBV) - a major player in the pathogenesis? *BMC Cancer*. 2020;20(1):34. [CrossRef]
35. Zhang W, Fang M, Dong D, et al. Development and validation of a CT-based radiomic nomogram for preoperative prediction of early recurrence in advanced gastric cancer. *Radiother Oncol*. 2020;145:13-20. [CrossRef]
36. Berenguer R, Pastor-Juan MDR, Canales-Vázquez J, et al. Radiomics of CT features may be nonreproducible and redundant: influence of CT acquisition parameters. *Radiology*. 2018;288(2):407-415. [CrossRef]
37. Mackin D, Fave X, Zhang L, et al. Measuring computed tomography scanner variability of radiomics features. *Invest Radiol*. 2015;50(11):757-765. [CrossRef]
38. Kim H, Park CM, Lee M, et al. Impact of reconstruction algorithms on CT radiomic features of pulmonary tumors: analysis of intra- and inter-reader variability and inter-reconstruction algorithm variability. *PLoS One*. 2016;11(10):e0164924. [CrossRef]
39. Midya A, Chakraborty J, Gönen M, Do RKG, Simpson AL. Influence of CT acquisition and reconstruction parameters on radiomic feature reproducibility. *J Med Imaging (Bellingham)*. 2018;5(1):011020. [CrossRef]
40. Zhao B, Tan Y, Tsai WY, et al. Reproducibility of radiomics for deciphering tumor phenotype with imaging. *Sci Rep*. 2016;6:23428. [CrossRef]
41. Ng F, Kozarski R, Ganeshan B, Goh V. Assessment of tumor heterogeneity by CT texture analysis: can the largest cross-sectional area be used as an alternative to whole tumor analysis? *Eur J Radiol*. 2013;82(2):342-348. [CrossRef]
42. Filograna L, Lenkowicz J, Cellini F, et al. Identification of the most significant magnetic resonance imaging (MRI) radiomic features in oncological patients with vertebral bone marrow metastatic disease: a feasibility study. *Radiol Med*. 2019;124(1):50-57. [CrossRef]
43. Degenhardt F, Seifert S, Szymczak S. Evaluation of variable selection methods for random forests and omics data sets. *Brief Bioinform*. 2019;20(2):492-503. [CrossRef]

Supplementary Table S1. Rad-score values of high, moderate, or low recurrence/metastasis risks in the training group (n = 124)

	High risk (n = 31)	Moderate risk (n = 56)	Low risk (n = 37)
Rad-score	(−1.63, −0.63)	(−0.53, 0.67)	(0.73, 1.81)
Recurrence/metastasis	24 (77.4%)	27 (48.2%)	7 (18.9%)
Relative risk	1.67 (high vs. moderate)	2.84 (moderate vs. low)	4.73 (high vs. low)
Rad-score *P*	<.001 (high vs. moderate)	<.001 (moderate vs. low)	<.001 (high vs. low)

Supplementary Table S2. Rad-score values of high, moderate, or low recurrence/metastasis risks in the validation group (n = 55)

	High risk (n = 6)	Moderate risk (n = 19)	Low risk (n = 30)
Rad-score	(−0.89, −0.60)	(−0.52, −0.02)	(0.04, 1.42)
Recurrence/metastasis	5 (83.3%)	11 (57.9%)	10 (33.3%)
Relative risk	1.78 (high vs. moderate)	1.50 (moderate vs. low)	2.67 (high vs. low)
Rad-score *P*	<.001 (high vs. moderate)	<.001 (moderate vs. low)	<.001 (high vs. low)

Supplementary Table S3. Rad-score values of high, moderate, or low recurrence/metastasis risks in the overall cases (n = 179)

	High risk (n = 37)	Moderate risk (n = 62)	Low risk (n = 80)
Rad-score	(−4.81, −0.60)	(−0.60, 0.18)	(0.22, 5.73)
Recurrence/metastasis	29 (78.4%)	33 (53.2%)	22 (27.5%)
Relative risk	1.62 (high vs. moderate)	1.93 (moderate vs. low)	3.12 (high vs. low)
Rad-score *P*	<.001 (high vs. moderate)	<.001 (moderate vs. low)	<.001 (high vs. low)